Tracing the role of endogenous carbon in denitrification using wine industry by-product as an external electron donor: coupling isotopic tools with mathematical modeling

R. Carrey[1*], P. Rodríguez-Escales[2,3], A. Soler[1], N. Otero[1,4]

1 Grup d'Mineralogia Aplicada i Medi Ambient, Dep. Mineralogia, Petrologia i Geologia Aplicada, Facultat de Ciències de la Terra, Universitat de Barcelona (UB), C/ Martí i Franquès s/n, 08028, Barcelona, Spain

2 Dept. of Civil and Environmental Engineering. Universitat Politècnica de Catalunya, Jordi Girona 1-3, 08034 Barcelona, Spain

3 Associated Unit: Hydrogeology Group (UPC-CSIC)

4 Serra Hunter Fellowship, Generalitat de Catalunya, Spain

*Corresponding author: raulcarrey@ub.edu

Abstract

Nitrate removal through enhanced biological denitrification (EBD), consisting of the inoculation of an external electron donor, is a feasible solution for the recovery of groundwater quality. In this context, liquid waste from wine industries (wine industry by-products, WIB) may be feasible for use as a reactant to enhance heterotrophic denitrification. To address the feasibility of WIB as electron donor to promote denitrification, as well as to evaluate the role of biomass as a secondary organic C source, a flow-through experiment was carried out. Chemical and isotopic characterization was performed and coupled with mathematical modeling. Complete nitrate attenuation with no nitrite accumulation was successfully achieved after 10 days. Four different C/N molar ratios (7.0, 2.0, 1.0 and 0) were tested. Progressive decrease of the C/N ratio reduced the remaining C in the outflow and favored biomass migration, producing significant changes in dispersivity in the reactor, which favored

efficient nitrate degradation. The applied mathematical model described the general trends for nitrate, ethanol, dissolved organic carbon (DOC) and dissolved inorganic carbon (DIC) concentrations. This model shows how the biomass present in the system is degraded to dissolved organic C (DOC_{en}) and becomes the main source of DOC for a C/N ratio between 1.0 and 0. The isotopic model developed for organic and inorganic carbon also describes the general trends of $\delta^{13}C$ of ethanol, DOC and DIC in the outflow water. The study of the evolution of the isotopic fractionation of organic C using a Rayleigh distillation model shows the shift in the organic carbon source from the WIB to the biomass and is in agreement with the isotopic fractionation values used to calibrate the model. Isotopic fractionations (ε) of C-ethanol and C-DOC_{en} were -1‰ and -5‰ (model) and -3.3‰ and -4.8‰ (Rayleigh), respectively. In addition, an inverse isotopic fractionation of +10‰ was observed for biomass degradation to DOC_{en}. Overall, WIB can efficiently promote nitrate reduction in EBD treatments. The conceptual model of the organic C cycle and the developed mathematical model accurately described the chemical and isotopic transformations that occur during this induced denitrification.

Keywords

Denitrification; stable isotopes; modeling; endogenous carbon; wine by-product; porous media

1 Introduction

Nitrate (NO_3^-) is one of the most common groundwater pollutants (Nolan, 2001; Puckett et al., 2011). NO_3^- contamination is originated either from diffuse (non-point) sources, linked to intensive use of synthetic and organic fertilizers and livestock, or from point sources such as septic system effluents. High NO_3^- ingestion affects human health, promoting cancer and producing methemoglobinemia in infants, also known as blue baby syndrome (Magee and

Barnes, 1956; Ward et al., 2005). Furthermore, an increase of NO_3^- can produce eutrophication of surface water bodies (Rivett et al., 2008; Vitousek et al., 1997). Consequently, the European Union has established a NO_3^- concentration threshold of 0.80 mM (50 mg/L) for human water supplies (Directives 98/83/CE, 91/676/CEE). This limit is exceeded in many aquifers worldwide because NO_3^- is highly mobile in groundwater and often persists in aquifers (He et al. 2011). Therefore, groundwater remediation has become a necessary strategy to prevent the public health and environmental impacts of NO_3^-. One of the most efficient treatments for removing NO_3^- involves enhanced biological denitrification (EBD) within the aquifer (Khan and Spalding 2004, Tartakovsky et al. 2002, Vidal-Gavilan et al. 2013). Denitrification is the process where NO_3^- is reduced to dinitrogen gas (N_2) by anaerobic facultative bacteria (Knowles 1982). In natural systems, denitrification is predominantly restricted by the availability of electron donors (Korom 1992). To overcome this natural limitation, biostimulation of heterotrophic denitrification by adding an organic carbon source is a feasible technique to reduce NO_3^- pollution in groundwater and wastewater (Vidal-Gavilan et al. 2013, Borden et al., 2011; Leverenz et al., 2010).

A number of studies have tested different soluble organic compounds, including pure compounds such as alcohols (ethanol, methanol), sugars (glucose, sucrose) and other organic compounds such as lactose, volatile fatty acids, acetic acid, propionate, and molasses (Fernández-Nava et al. 2008, Gómez et al. 2000, Peng et al. 2007). Recently, there has been increasing interest in alternative sources of organic carbon solid compounds such as palm tree leaves, compost or saw dust to promote water remediation for different pollutants (Grau-Martínez et al., 2017; Schipper and Vojvodic, 2000; Trois et al., 2010). The use of by-products from the food industry as organic carbon sources may provide an economical alternative solution while providing waste recycling. Furthermore, these industrial by-products may provide both an easily accessible carbon source and micronutrients. In this context, liquid waste from wine industries may be a feasible reactant to enhance heterotrophic

denitrification. The proposed wine industry by-product (WIB) where organic carbon is mainly composed of ethanol (95%), and is generated during brandy distillation, after which residual liquid in the container is discarded. The liquid waste is usually treated in a wastewater treatment plant at an elevated cost for the wine companies (Petta et al., 2017).

An essential concern in EBD is to design an efficient feeding strategy that can avoid the production of undesirable compounds such as nitrite (NO_2^-) and nitrogen oxides (Vidal-Gavilan et al. 2014) as well as minimize the risk of bioclogging due to denitrifier biomass growth (Rodríguez-Escales et al. 2016b). One of the key factors controlling these risks is the amount of dissolved organic carbon (DOC) inoculated. It should be enough to guarantee a sufficient NO_3^- reduction, but it should not exceed the stoichiometric requirements of the reaction to avoid undesirable reactions such as sulfate reduction. The DOC inoculated is commonly calculated by considering only the organic carbon injected into the system. However, as the denitrifier biomass grows and dies, a new carbon pool, formed by dead and lysed cells, appears in the system and has the potential to become a new source for denitrification (Carrey et al. 2014a, Rodríguez-Escales et al. 2016b, Rodríguez-Escales et al. 2014, Torrentó et al. 2011). The total denitrification rate is the combined reduction of NO_3^- due to the different organic carbon sources, including external, or exogenous, and internal, or endogenous, sources. Normally, endogenous respiration is slower than exogenous; it does not depend on the organic substrate availability (Orozco et al. 2010) and thus becomes more important when the external carbon source has been exhausted. The incorporation of endogenous carbon into the calculation of the C/N (carbon/nitrogen) ratio will reduce the amount of external DOC, decreasing the cost of EBD as well as minimizing the risk of bioclogging in the system.

The role of endogenous carbon in the denitrification rate cannot be addressed only by traditional hydrochemistry. In addition to microbiological molecular tools, mathematical modeling with stable carbon isotopic data is a powerful tool to understand the carbon cycle during denitrification. Furthermore, incorporating isotopes into the biogeochemical model

allows the determination of the isotopic fractionation (ε) of complex processes that cannot be analyzed using traditional equations (Abe and Hunkeler 2006, van Breukelen 2007, van Breukelen and Prommer 2008). Typically, ε is calculated as a Rayleigh distillation process (Mariotti et al., 1981) (Eq. 1) and it is expressed in per mil units (‰):

$$Ln\left(\frac{R_t}{R_0}\right) = (\varepsilon) * Ln(\frac{C_t}{C_0}) \qquad (1)$$

where C_0 and C_t are the initial and residual concentration at time *t* (ML^{-3}), respectively, and R_0 and R_t are the isotopic ratios (ratio of heavy to light isotopes) at the initial time and at time *t,* respectively, that are calculated according to Eq. 2:

$$R = \left[\left(\frac{\delta}{1000}\right) + 1\right] \qquad (2)$$

where δ is the isotopic composition in per mil units (‰). The term ε is calculated from the slope of the linear regression analysis in the double-logarithmic plot of $Ln(R_t/R_0)$ versus $Ln(C_t/C_0)$ according to Eq. 1. Following the recommendations of Coplen (2000), ε will be expressed as $\varepsilon^{i}E_{P/Q}$, where $\varepsilon^{i}E$ is the isotopic fractionation for the element E (where *i* is the heavier isotope) between substances P (product) and Q (reactant) for a specific transformation. To facilitate comparison with literature values, ε is expressed in per mil units (‰).

The main goal of this work is to evaluate, by coupling carbon isotopes and modeling, the role of endogenous carbon in denitrification using WIB as a carbon source. The side objectives are i) to evaluate the viability of using WIB to remediate NO_3^- contaminated water using different C/N ratios, focusing on the generation of undesirable compounds such as NO_2^-, and ii) to study the feasibility of using the Rayleigh equation to determine the isotopic fractionation of the different carbon pools. To achieve these goals, a flow-through experiment was set up, and chemical, isotopic and biological characterization was performed. In addition, a complete model integrating the hydrochemistry and the carbon isotope signatures was developed.

2 Methodology

2.1 Experimental set-up

A flow-through glass column was built to simulate a 1D lab-scale model and installed in a temperature-regulated chamber (Fig. 1 in Supporting Information). The experimental system included a 2 L inflow water reservoir, a 70 cm long and 8 cm diameter glass column, and a 500 mL outflow reservoir, all of them connected by Tygon® R-3603 tubes. Synthetic water flowed through the column from the bottom to the top. Inflow and outflow rates were set constant at an average rate of 360 mL/d using a peristaltic pump (Reglo Digital peristaltic micropump, ISMATEC) connected to both ends of the column. The resulting hydraulic residence time is about 5 days. Eight sampling points were established: one at the inflow water reservoir (I), six across the glass column at 10 cm intervals (sampling points 1 to 6), and one at the outflow (O).

The column was filled with sterilized silica balls (5 mm in diameter) to obtain an unreacted and homogeneous matrix. Synthetic water was prepared 3 times during the experiment (at days 0, 30 and 60). Table 1 presents a summary of the average theoretical concentrations of anions and cations of the synthetic medium. The NO_3^- concentration varied slightly among different containers. The first water container used (day 0 to day 30) had 1.52 mM of NO_3^-, the second container (from day 30 to day 60) had 2.02 mM of NO_3^-, and the last container (from day 60 to 80) had 1.82 mM of NO_3^-. The concentrations of NO_2^-, NH_4^+, Fe, Mn and DOC in the three inflow water containers were below the detection limits (<$2.2x10^{-3}$ mM, $5.5x10^{-3}$ mM, <$8.9x10^{-5}$ mM, <$1.8x10^{-5}$ mM and <0.04 mM, respectively).

The flow-through experiment ran at common average Mediterranean aquifer temperature (15°C). A control experiment with no carbon addition was run for 1 month before starting the biostimulation. A tracer test was performed prior to the beginning of the experiment using a conservative tracer to determine the main transport properties of the column. Tracer test results showed that the porosity was 0.6 and the dispersivity coefficient was $5x10^{-3}$ m (results not shown).

The injections of the WIB were performed through 4 injection points located at sampling point #2, near the bottom of the column (see Fig. 1 in supporting information). During the experiment, four different stages with varied C/N molar ratios were tested (which represent the amount of injected C versus the N mass-flux across the column within an injection interval of 4 days). Initially (stage I, from days 0 to 20) the C/N molar ratio was approximately 7.0, corresponding to 18.7 mmol of C per injection (14 mL of WIB). From day 20 to day 40 (Stage II) the C/N ratio was about 2.0 (4 mL of WIB, corresponding to 5.9 mmol of C per injection). From day 40 to day 60 (Stage III) the C/N molar ratio was close to 1.0 (2 mL of WIB, 2.7 mmol of C per injection). Finally, from day 60 to day 80 WIB was not injected in the flow-through experiment.

2.1.1 Analytical methods

During the experiment, 3 inflow water and 95 outflow water samples were collected over 80 days. In addition, 3 column profiles were conducted (17, 37 and 53 days after the first injection), consisting of 7 samples each (one from the inflow water and one from each monitoring point along the column). The outflow of the column was sampled every 12h until day 24 and daily afterwards. Obtained samples were immediately filtered through a 0.2 µm Millipore® filter and stored at 4°C for further analysis. Chemical parameters were determined by standard analytical techniques: major anions (Cl^-, NO_3^-, NO_2^-, SO_4^{2-}) by high-performance liquid chromatography (HPLC) using a WATERS 515 HPLC pump with IC-PAC Anion columns and a WATERS 432 and UV/VIS KONTRON detectors; alkalinity (HCO_3^-) by titration (METROHM 702SM Titrino); NH_4^+ by colorimetry; and non-purgeable dissolved organic matter (NPDOC) by organic-matter combustion (TOC 500 SHIMADZU). For ease of reading, NPDOC will be expressed as DOC hereafter. The uncertainties in these measurements were determined to be approximately 5% for NO_3^-, NH_4^+ and SO_4^{2-}; 10% for NO_2^-; 0.08 mM for HCO_3^-; and 0.25 mM for

DOC, while the pH error was 0.02 pH units. Detection limits were 0.003 and 0.004 mM for NO_3^- and NO_2^- respectively and 0.08 mM for DOC.

The isotopic characterization included the carbon isotopic compositions of DIC ($\delta^{13}C_{DIC}$), DOC ($\delta^{13}C_{DOC}$), ethanol ($\delta^{13}C_{EtOH}$), and biomass ($\delta^{13}C_{Bm}$). The $\delta^{13}C$ analysis for DIC was performed using a Thermo Scientific GasBench II-Mat 253, while the $\delta^{13}C_{DOC}$ was analyzed by HPLC-IRMS and $\delta^{13}C_{EtOH}$ was measured via GC-IRMS, with both analyses performed with a Delta V ADVANTAGE instrument, Thermo-Finnigan, Bremen, Germany. The $\delta^{13}C_{Bm}$ was determined using a Carlo Erba EA-Finnigan Delta C IRMS. The isotope ratios were calculated using international and internal laboratory standards. Notation is expressed relative to the international V-PDB (Vienna Peedee Belemnite) standard for $\delta^{13}C$. The reproducibility (1σ) of the samples, calculated from standards systematically interspersed in the analytical batches, was ±0.2‰ for $\delta^{13}C_{DIC}$, ±0.2‰ for $\delta^{13}C_{EtOH}$, 0.3‰ for $\delta^{13}C_{DOC}$, and ±0.3‰ for $\delta^{13}C_{Bm}$. Chemical and isotopic analyses were performed at the Centres Científics i Tecnològics of the Universitat de Barcelona.

2.1.2 Microbiological analysis

During the experiment, the denitrifying population was quantified using the most probable number (MPN) method published by (Saitoh et al. 2003). In addition, the total aerobic heterotrophic population was obtained using the miniaturized MPN method as described in Wrenn and Venosa (1996). Five milliliters of water was removed from three sampling ports 1, 2 and 3 (Fig. 1 in supporting information) along the column. Samples were processed within 6 h of collection. Sampling was performed on days 16, 24, 31, 44, 52, 61 and 68. To estimate the population density of the denitrifying bacteria, the water sample was diluted up to a maximum of $1/10^{12}$. Nine 0.25 mL replicates of each dilution were placed in Eppendorf vials with 0.25 mL sterilized nutrient broth (NB) medium. The NB solution contained 6 g/L beef extract, 10 g/L peptone, 2 g/L $NaNO_3$, 0.05 g/L $NaNO_2$, 2 g/L agar, and 2.5 g/L HEPES. The pH of the NB was

adjusted to 7.0 using a 0.1 M NaOH. Eppendorf vials containing the diluted sample and NB were individually sealed with 1 mL overlaying solution containing 5 g/L agar and 8 g/L gellan gum to preserve the N_2 bubbles formed by the denitrifying bacteria. To calculate the population density of the heterotrophic bacteria, the diluted samples were added to microtiter plates using sterilized tryptic soy broth (TSB) solution as a culture medium. Twenty-five microliters of TSB was placed in each well and mixed with 25 µL diluted sample. Eight replicate wells per dilution were constructed. The positive tests were used to calculate the MPN of the heterotrophic organisms per milliliter of water.

2.2 Carbon flow conceptualization and model construction

2.2.1 Conceptual model of carbon flow in denitrification

The carbon flow in denitrification was conceptualized with four main carbon pools (Fig. 1). The first pool was the external carbon added as an organic carbon source, in this case the wine industry by-product (ethanol or EtOH). The second pool was the biomass material, which was composed of all the microbiological compounds within it, including live cells, dead cells, and external polycarbonate substances (EPS), as described in Carles-Brangarí et al. (2017). The third pool was the organic C from biomass degradation (DOC_{en}). Different processes contributing to the DOC_{en} pool could occur -such as cell lysis through hydrolysis and the production of storage compounds as poly-beta-hydroxybutyrate (PHB)- which could be used as endogenous carbon sources when the external carbon was limited. Finally, the fourth pool was the DIC. This carbon pool was the sum of inflow water DIC and the oxidation of both the external organic carbon (ethanol) and the endogenous carbon (DOC_{en}). Note that inorganic carbon was equilibrated with pH and can include different species depending on the hydrochemistry of the water, including $CO_{2(aq)}$, HCO_3^-, and CO_3^{2-}. The endogenous carbon

source could also be incorporated, again, into new biomass, but we neglected this process to simplify the model.

2.3 Model construction

2.3.1 Coupling the denitrification model with carbon isotopic data

Table 2 shows the main rates of denitrification (1-3); they describe the same processes as Fig. 1. As most of the WIB was composed of ethanol, we predicted the next general reaction for denitrification using WIB:

$$0.943\ C_2H_5OH + 1\ NO_3^- + 0.489\ H^+ = 0.273\ C_5H_7O_2N + 0.364\ N_2 + 0.511\ HCO_3^- + 1.864\ H_2O \quad \text{(Eq. 3)}$$

Eq. 3 was determined as (Rittmann and McCarty 2001) and was used to determine (i) the portion of the electron donor used for cell synthesis during denitrification (Y_h), which was 0.724 C-biomass/C-ethanol, and (ii) the portion of electron acceptor (NO_3^-) consumed by substrate oxidation (Q), which was 0.53 mol N-NO_3^-/mol C-ethanol. The biomass concentration, [X] in Table 2, was conceptualized as having an average chemical composition of $C_5H_7O_2N$ (Porges et al. 1956). The stoichiometric relationship between NO_3^- and DOC_{en} (S) was assumed to be 0.92 mol NO_3^-/mol DOC_{en}, following (Rodríguez-Escales et al. 2014).

The role of NO_2^- as an electron acceptor in the model was not considered because its accumulation was not representative during the experiment. It was not detected in the outflow of the experiment during most part of the experiment (it only was remarkable up to day 5), neither in the different profiles sampled at (days 17, 37 and 53).Therefore, the model was considered to be only one reduction step from NO_3^- to N_2 gas. The potential accumulation of NO and N_2O was also discarded. The presence of easily degradable C substrates has been reported to increase denitrification and may decrease the N_2O/N_2 ratio (Weier et al., 1993, Welti et al., 2012). Despite N_2O and NO not being determined, the periodic addition of easily

degradable organic C favors a rapid denitrification; therefore, the N_2O generation was assumed to be limited following Rivett et al. (2008) and Tallec et al. (2008).

The oxidation of injected ethanol by dissolved oxygen in the inflow water was neglected. This assumption was based on the calculated organic carbon consumption by dissolved oxygen in the inflow water, which showed values between 0.1% (C/N = 7) and 4% (C/N = 0.6) of ethanol injected (results not shown). Moreover, preliminary models considering the instantaneous reduction of oxygen showed that oxygen was consumed within the first 5 cm of the column (results not shown).

The carbon isotope geochemistry was modeled considering the same processes described in Fig. 1. The main rates are shown in Table 2. The actual model is based on and extended from previous work (Rodríguez-Escales et al. 2014). The extension was mainly based on the incorporation of the DOC_{en} pool into the system. We followed the same simplifications as Rodríguez-Escales et al. (2014): we assumed that the isotopic effect of the external organic carbon was the apparent effect of the overall internal metabolism; furthermore, we did not consider special fractionation of carbon into biomass and inorganic carbon. The carbon isotope geochemistry was simulated by adding the "^{12}C" and "^{13}C" of each carbon species (ethanol, DIC, DOC and biomass) as a separate imaginary solute to the model. The exact concentrations of both isotopes were calculated from the inflow and WIB carbon isotope signature (Table 1). The $\delta^{13}C$ of heterotrophic biomass in other studies fell within -10.3 to -25.4‰ for *Pseudomonas aeruginosa* (Blair et al. 1985, Coffin et al. 1990). In the present experiment, the initial value $\delta^{13}C_{Bm}$ used in the model was -20‰.

2.3.2 Codes used

The PHT3D model code (v. 2.17) (Prommer and Post 2010) was used to simulate the evolution of water hydrochemistry as well as the stable isotopes evolution during enhanced denitrification in the column. This model code couples the transport simulator MT3DMS

(Zheng and Wang 1999) and the geochemical model PHREEQC-2 (Parkhurst and Appelo 1999) based on a sequential split-operator technique. Regarding the solute transport, MT3DMS uses the traditional advection-dispersion equation:

$$\phi \frac{\partial C_i}{\partial t} = -q\ \nabla C_i + \phi \nabla(\mathrm{D} \nabla C_i) \qquad (4)$$

where D is the dispersion tensor [L^2T^{-1}]; q is Darcy's velocity ([LT^{-1}], which is related to the hydraulic conductivity [LT^{-1}] and water gradient [-]); and ϕ is the porosity [-]. Both the velocity and the dispersion tensor were taken from the experimental tracer test (see Section 2.1). The 1D model was discretized into 70 elements of 1 cm length. The time discretization was selected to satisfy the Peclet and Courant criteria. Dispersive transport was computed according to the third-order total variation diminishing scheme. Since the PHT3D reaction module uses the original PHREEQC-2 database syntax, equilibrium and non-equilibrium reaction chains can be defined. For reactions in equilibrium, the constants were taken directly from the general PHREEQC database. Kinetic processes reactions such as ethanol degradation and bacterial growth/decay (equations 1-3 from Table 2), not being part of the standard database, were incorporated into the module in the form of BASIC routines, as explained in Rodríguez-Escales et al. (2014) and Carrey et al. (2014b). Calibration process was performed by hand using the experimental information: ethanol, nitrate, DOC concentrations, as well as carbon isotope information.

3 Results and Discussion

The bulk dataset from the flow-through experiment is provided as Supporting Information (Table SI-1).

3.1 Denitrification enhanced by WIB injection and NO_2^- accumulation

During the control experiment, no NO_3^- variations were observed in the outflow water compared with the inflow water (data not shown). This finding indicated that in the main

experiment, nitrate reduction was promoted by the oxidation of the external organic carbon (WIB-ethanol). In the main experiment, NO_3^- reduction started quickly (day 5, 2nd injection), reaching complete NO_3^- attenuation on day 6 (Fig. 2). As stated above, the WIB was the only source of electron donors. Since the contribution to biomass of the inflow water and the silica balls can be considered negligible, the WIB was also the main source of denitrifier biomass. Therefore, the WIB was able to effectively stimulate its own microorganisms. Complete nitrate degradation occurred on day 6 (Fig. 2). This lag time is similar to that observed in analogous column experiments using ethanol as a carbon source, groundwater and aquifer sediment as filling material (Vidal-Gavilan et al. 2014). This finding may indicate that WIB could achieve at least the same degradation rates in natural systems since it would add to the system a source of denitrifier biomass.

The initial decrease of NO_3^- was coupled with an important peak of NO_2^- concentration in the outflow in the first days of the experiment (up to 1.7 mM at day 5) (Fig. 2c). This first initial NO_2^- accumulation lasted for 48 h after the second injection and thereafter decreased to below the detection limit from day 11 to day 65. A slight NO_2^- accumulation (up to 0.1 mM) was again observed from day 65 to 80. NO_2^- accumulation is explained by the incomplete reduction of NO_3^-. Other processes that can produce NO_2^- accumulation, such as dissimilatory nitrate reduction to ammonia (DNRA), were dismissed because NH_4^+ was not detected in the outflow water. Therefore, denitrification was considered the main reaction that affects NO_3^- and NO_2^- variation during the experiment. NO_2^- accumulation is due to the repression of the production of NO_2^- reductase (Kraft et al., 2011; Strohm et al., 2007). The enzymatic repression is controlled by several factors such as the organic C type, pH and evolution of the microbial population involved in the reaction (Glass and Silverstein 1998, Gómez et al. 2000, Martin et al. 2009). The organic C from WIB was mainly ethanol, which produces low NO_2^- accumulation during denitrification (Carrey et al. 2014a, Gómez et al. 2000, Martin et al. 2009). The pH measured in the outflow water was within the optimum range for NO_2^- reduction (6.1 to 7.2)

(Glass and Silverstein 1998). Hence, the main factor controlling the high NO_2^- concentration due to enzymatic repression seems to be microbial evolution. The NO_2^- accumulation diminished over time when the microbial population was able to overtake the lag in NO_2^- reduction produced due to reductase repression. The denitrifying microbial population inside the reactor increased from negligible values before the WIB injection up to $4.6x10^5$ MPN cells/mL of denitrifiers measured at day 16 (after complete NO_3^- attenuation was reached). In similar flow-through experiments using natural sediment and groundwater, initial microbial population ranged from $4.4x10^0$ to $5.5x10^1$ MPN cells/mL (Carrey et al., 2014, Vidal-Gavilan et al., 2014). In the above-mentioned experiments, the initial NO_2^- accumulation was related with enzymatic repression of NO_2^- reductase of denitrifiers, and was favored by the low bacteria population at the initial stage. Therefore, it is reasonable to assume that in the initial period, the low microbial population in the system was the critical factor that favored NO_2^- accumulation. A second NO_2^- accumulation peak was detected at the end of the experiment. After day 65 (9 days after the last WIB injection), the NO_2^- concentration ranged from 0.06 to 0.1 mM. In this last period, once carbon addition was stopped, the availability of organic carbon in the system was progressively reduced, producing inefficient denitrification and leading to NO_2^- accumulation (from 0.02 to 0.1 mM).

3.2 Denitrification kinetic modeling

Changes in the C/N ratio did not prevent complete NO_3^- reduction, which indicates that after the initial lag phase (6 days), complete attenuation could be maintained at the outflow of the reactor. On one side, denitrification produced an increase of dispersivity, which enhanced the optimal consumption of carbon; on the other side the biomass growth favored endogenous carbon production. The first point is demonstrated by the biogeochemical model and biomass monitoring, and the second point is discussed in Section 3.3.

The biogeochemical model showed that dispersivity and, thus, heterogeneity increased over time in the experiment. Although we used silica balls as a filling material to represent a

homogeneous porous medium, this material did not allow biomass attachment, favoring its migration across the porous medium (biological material was continuously observed at the outflow of the experiment). Thus, the system became more heterogeneous, and it was not possible to use the dispersivity value obtained in the initial tracer test ($1x10^{-3}$ m) in the biogeochemical model. Therefore, this parameter was re-calibrated using the biogeochemical data; we considered the initial peaks of ethanol as well as the nitrate recuperation from day 65 on. Furthermore, the fitting of dispersivity was constrained by the absence of nitrate at the outflow of the column beginning on day 6. The fitting process showed that it was not possible to define a unique representative dispersivity value for the whole experiment. Hence, two dispersivity values were combined: the one obtained for the initial days (1-20 days, $9.8x10^{-2}$ m) and the one obtained for the last days (65-80 days, $3.5x10^{-1}$ m); the change of dispersivity in the model was applied on day 20. Note that dispersivity increased by approximately 100-fold during the first days and 3.6-fold during the rest of the experiment. Changes in dispersivity due to biomass growth have been observed in previous works (e.g. Delay et al. 2013, Rodríguez-Escales et al. 2016a, Taylor and Jaffé 1990). In particular, Taylor and Jaffé (1990) observed changes in dispersivity in the range of 100 and 1000, which are in agreement with the present results. When dispersivity is higher, the system is more efficient because it facilitates nutrient spread along the column (Rodríguez-Escales et al. 2016a). This hypothesis of heterogeneity was also supported by the variation of MPN counts of heterotrophic and denitrifying bacteria in the column profiles. In general, the higher heterotrophic and denitrifying populations were observed in the top of the column and during the period without WIB injection (Fig. 2 in supporting information). A low C/N ratio has been shown to favor the poor flocculation, settleability and dewaterability of the flocs (Ye et al., 2011, Cetin and Erdincler 2004). These characteristics favored the migration of insoluble biological material across the column, inducing heterogeneity, which results in higher dispersivity.

Once the transport model was calibrated, the kinetic parameters for the biogeochemical model were determined. The best values determined by manual calibration are shown in Table 3. The model was able to reproduce the experimental data of NO_3^-, ethanol (Fig. 2), DIC and DOC (Fig. 3). Note that outflow DOC represents the sum of ethanol and DOC from the biomass material (see Fig. 1). The fitted parameters were of the same order of magnitude as the literature values (Table 3), except for K_{max}, which was one order of magnitude higher than reported values, indicating a higher reactivity of the electron donor. This difference may be because the experimental values were obtained under more favorable conditions, such as biological activity, than those previously reported from field studies. Hence, although the kinetic parameters obtained in the present study cannot be directly extrapolated to the field scale, the developed kinetic model was essential for identifying and estimating changes produced in the hydraulic parameters related to biomass growth, which can modify the behavior of the treatment efficiency over time. Furthermore, the biogeochemical model is the basis for the isotopic model of C, which provided information about the source of electron donors throughout the experiment, as described in the next sections.

3.3 Carbon fate and isotopic fractionation during denitrification

The periodic injection of WIB sustained denitrification even though the organic carbon source was drastically reduced from a C/N molar ratio of 7.0 to zero. This change indicated that WIB was not the only source of electron donors in the system. As indicated by the conceptual model (Fig. 1) both the DOC periodically injected as WIB (mainly ethanol), and the organic carbon derived from biomass (DOC_{en}) contributed to the DOC pool. The measured DOC in the outflow represents the sum of ethanol not consumed during denitrification and DOC_{en}. Fig. 3 shows the experimental and modeling results for ethanol (Fig. 3a) and DOC_{en} (Fig. 3b). The model captured the general tendency of the experimental values, indicating that the simplifications considered in the conceptual model were adequate. Fig. 3d shows the

calculated percentages of DOC_{en} and ethanol sources throughout the experiment. The importance of ethanol decreased considerably when the C/N ratio was modified to 2.0 (Fig. 3c). This change is explained by the decreasing of the C/N ratio by itself; moreover, at that point, there was a sizable biomass population, which allowed the formation of endogenous carbon (Fig. 2 in supporting information). During the first two C/N ratio stages, the ethanol concentration matched the DOC in those samples with DOC >8.5 mM, indicating that ethanol was the main DOC source (Fig. 3a). However, for samples with DOC <8.5 mM, only approximately 50% of the DOC could be attributed to ethanol. Hence, even with a higher C/N ratio than the stoichiometric values, the biomass grown in the system started to be degraded to DOC_{en}, contributing to the DOC pool. The role of DOC_{en} became more important as the C/N ratio decreased, especially with a C/N ratio of 1.0, where for some samples (day 43), up to 70% of the DOC was derived from DOC_{en} (Fig. 3b). Finally, during the period with no WIB injection, the ethanol concentration was below the detection limit in all samples, and hence, the outflow DOC was exclusively derived from DOC_{en} (Fig. 3b). Thus, during an induced denitrification treatment, biomass can be a relevant source of organic carbon, acting as buffer for denitrification when the concentration of the electron donor is restricted.

The oxidation of both ethanol and endogenous carbon produced variations in DIC concentration (Fig. 3c and Table 2). The inflow water had 0.51 mM of DIC, whereas the outflow had 0.91 mM beginning with the first sampling. This initial DIC increase is attributed to the dissolution of atmospheric CO_2 due to the re-equilibrium. Therefore, for the model, we considered this value (0.91 mM) as the initial concentration, assuming that DIC was equilibrated with $CO_{2(atm)}$ ($P_{CO2,eq}$ = $3.5 \cdot 10^{-4}$ atm). The DIC content was modeled taking into account the oxidation of ethanol and DOC_{en}. The model describes the general tendency of DIC (Fig. 3c), although some initial oscillations were not well described. Discrepancies could be produced by further variations of the CO_2 re-equilibrium in the reactor, which were not considered in the model.

The study of the isotopic compositions of the different C compounds provided additional information about their roles during denitrification and was also useful for calibrating the model. Fig. 4 shows the experimental and modeling results of the $\delta^{13}C$ of the different pools: $\delta^{13}C_{EtOH}$ (Fig. 4a), $\delta^{13}C_{DOC}$ (Fig. 4b), and $\delta^{13}C_{DIC}$ (Fig. 4c). The isotopic fractionation values (ε) considered in the model were $\varepsilon^{13}C_{DIC/EtOH}$, $\varepsilon^{13}C_{Bm/EtOH}$, $\varepsilon^{13}C_{DOCen/Bm}$, and $\varepsilon^{13}C_{DIC/DOCen}$, and the calibrated values are shown in Table 3 and included in the conceptual model for carbon flow represented in Fig. 5. The results of the model showed that there was a low-normal isotopic fractionation in the transformation of ethanol to biomass ($\varepsilon^{13}C_{Bm/EtOH)}$ = -1‰). This would imply that with no other reactions and neglecting the initial biomass, the $\delta^{13}C$ of the produced biomass should be approximately -27‰ (initial $\delta^{13}C_{EtOh}$ was -26.1‰). This value is in agreement with the isotopic value measured in the biomass sampled in the outflow water (mean $\delta^{13}C_{Bm}$ of -27.9‰ ± 1.2‰). The next step is the biomass transformation to DOC_{en} (Fig. 5). The results of the model indicated an inverse fractionation in this process with an $\varepsilon^{13}C_{DOCen/Bm}$ of +10‰. This value should match the measured $\delta^{13}C_{DOC}$ during stage IV (no injection) when the only DOC source was DOC_{en}. The measured $\delta^{13}C_{DOC}$ during stage IV had an average value of -22.8‰ ± 0.6‰, which is higher than that of the biomass, in agreement with an inverse fractionation. However, as the biomass is degraded, it should show a lower isotopic composition, but this was not observed. This could be explained by a lower rate of transformation of biomass into DOC_{en} compared to the rate of transformation of ethanol into biomass, as a result the ^{13}C of biomass was mainly governed by the fractionation between biomass and ethanol.

Finally, the evolution of $\delta^{13}C$-DIC was modeled and compared with experimental data (Fig. 4c). The first process affecting DIC concentration and $\delta^{13}C$ is the equilibrium with atmospheric CO_2. This produces a decrease from the initial $\delta^{13}C_{DIC}$ of -8.1‰ in the inflow water to $\delta^{13}C_{DIC}$ of -20‰ in the outflow water, coupled with an increase in DIC from 0.5 mM to 0.9 mM and an increase in pH from 5.6 to 7.0. During CO_2 dissolution, $^{12}CO_2$ is preferentially

incorporated into the liquid (Abongwa and Atekwana, 2013). The variations in pH can produce the transformation of H_2CO_3 to HCO_3^-, increasing DIC and decreasing $\delta^{13}C_{DIC}$, as observed (Fig. 4c). The isotopic fractionation was calculated for the oxidation of ethanol and DOC_{en}. Both processes showed normal fractionations: $\varepsilon^{13}C_{DIC/EtOH}$ = -1‰ and $\varepsilon^{13}C_{DIC/DOCen}$ = -5‰ (Fig. 5). The model adjusted well the DIC concentration and isotopic composition, especially for stages I and II, except the initial values before the first injection.

3.4 Comparing isotopic fractionation: modeling versus Rayleigh equation

The isotopic fractionation (ε) related to organic C oxidation was calculated using the Rayleigh equation. Since the injection strategy was periodic, the initial organic C concentration (C_0) was not constant. In addition, two different sources of organic C were considered (ethanol and DOC_{en}); therefore, the initial $\delta^{13}C_{DOC}$ (R_0) was also variable over time. Hence, two hypotheses with different initial C_0 and R_0 values were defined. The first hypothesis (stages I, II and III) considered ethanol the main carbon source and the second hypothesis (stages III and IV) considered DOC_{en} the main carbon source. The ε values obtained represent the transformations of ethanol ($\varepsilon^{13}C_{EtOH}$) and DOC_{en} ($\varepsilon^{13}C_{DOCen}$) to both products of the reaction (DIC and biomass), but each specific transformation could not be described. For the first hypothesis, $\varepsilon^{13}C_{EtOH}$ was calculated assuming that NO_3^- was reduced using only ethanol as an electron donor. Hence, C_0 for each sample was determined as the sum of the outflow ethanol concentration and the ethanol consumed to reduce nitrate, calculated with Eq. 3. The R_0 was the initial $\delta^{13}C$ of WIB-ethanol (-26.1‰). Finally, C_t and R_t were the ethanol concentration and $\delta^{13}C_{EtOH}$, respectively, measured in the outflow. The obtained $\varepsilon^{13}C_{EtOH}$ for each stage decreased (in absolute values) from -3.1‰ (stage I) to -2.2‰ (stage II) to -0.8‰ (stage III) (Fig. 6a). This progressive decrease can be explained by an increasing influence of the DOC_{en} that was being oxidized to reduce nitrate. Therefore, during stage III, the evolution of the $\varepsilon^{13}C_{EtOH}$ (close to

0‰) represents no isotopic change in ethanol, revealing DOC_{en} as the main source of organic carbon, in agreement with the model results.

For the second hypothesis (the main source of C is DOC_{en}), data from stages III and IV (C/N = 0.6 and non-feeding) were used. C_0 was calculated as the sum of the DOC measured in the outflow and the DOC consumed to reduce nitrate, calculated from the stoichiometric C/N ratio reported for endogenous C oxidation (1 mol of C to reduce 0.92 mol of NO_3^-, as described in Rodríguez-Escales et al., 2014) and assuming no contribution from ethanol. The $\delta^{13}C$ used to calculate R_0 during stage III was the average of $\delta^{13}C_{Bm}$ determined in the outflow during stage III (-28.6‰), whereas for stage IV, the initial $\delta^{13}C_{DOCen}$ was considered the final measured $\delta^{13}C_{Bm}$ value (-28.9‰). The results for stage III fit well with an isotopic fractionation of -4.8‰, slightly higher (in absolute value) than the isotopic fractionation calculated for ethanol during stage I and similar to the value used in the model calibration (-5‰) (Fig. 6b). However, in the Rayleigh model, the *y*-axis intersection of the regression line must be close to 0 (that is, the initial point when $C_0 = C_t$ and $R_0 = R_t$), and the regression line intersects the y-axis at a remarkably high value. One feasible explanation is that the assumption of no fractionation in the incorporation of biomass into DOC_{en} is not correct. The trend of the regression line suggests a higher $\delta^{13}C$-DOC_{en} than the value of the precursor biomass, indicating an inverse isotopic fractionation in the biomass degradation to DOC_{en}. This condition is in agreement with the modeled $\varepsilon^{13}C_{DOCen/Bm}$ (Fig. 5). Samples from stage III showed a good correlation in a $Ln(C_t/C_0)$ vs. $Ln(R_t/R_0)$ plot, suggesting that the initial $\delta^{13}C_{DOCen}$ remained almost constant during stage III. In contrast, during stage IV, when WIB injection stopped, biomass formation was limited, and a variation in the $\delta^{13}C_{Bm}$ to more depleted values and different R_0 should be expected. Thus, the DOC_{en} source was variable, and samples did not show a clear trend when the Rayleigh distillation equation was applied. The model is able to overcome this limitation as it takes into account the products of the reaction ($\delta^{13}C_{DIC}$) that can help depict the evolution of initial $\delta^{13}C_{DOCen}$ as the reaction is being repressed. Therefore, the isotopic model can be a

useful approach to obtaining isotopic fractionation in complex systems such as organic C transformation during induced denitrification. In general, the isotopic fractionation values obtained using the Rayleigh equation agree with values of the isotopic model. The presence of multiple sources (DOC_{en} and ethanol) in a flow-through system increases the uncertainty of the isotopic fractionation calculated using only the Rayleigh equation.

Overall, the isotopic fractionation study has confirmed the important role of DOC_{en} in the degradation of nitrate observed in the model. The periodic injection of WIB can supply enough DOC_{ex} to achieve complete nitrate attenuation as a result of constant biomass degradation to DOC_{en}. A better knowledge of the C cycle, taking into account all the organic C sources, is crucial to the design of efficient field-scale biostimulation strategies to avoid the generation of undesirable compounds or inefficient nitrate degradation. In this context, the present work presents a simplified conceptual model of C transfer during induced denitrification at the lab scale that is able to quantify the role of endogenous organic C when C/N ratios are decreased.

4 CONCLUSIONS

The viability of periodic injections of WIB to remove NO_3^- from water was demonstrated in a flow-through experiment using a variable C/N molar ratio. Complete nitrate reduction in the experiment was driven by the oxidation of two organic carbon sources: i) organic carbon from WIB (ethanol) and ii) organic carbon from biomass degradation (endogenous). The results of the mathematical model showed how biomass degradation became the main source of DOC measured in the outflow water for low C/N ratios (1.0 and 0). The study of the isotopic fractionation of the different C species (ethanol, DOC and DIC) confirmed the shift in the source of organic C. The isotopic fractionations of the different organic carbon species obtained using the mathematical model and the Rayleigh equation showed comparable values. The isotopic fractionations (ε) of C-ethanol and C-DOC_{en} were -1‰ and -5‰ (model) and -3.3‰ and -4.8‰ (Rayleigh), respectively. In addition, an inverse isotopic fractionation of

+10‰ was observed for biomass degradation to DOC_{en} (model). The Rayleigh model showed uncertainties when multiple sources of organic C were present or when biomass was being depleted. The obtained results highlight the importance of understanding the role of the endogenous organic carbon for the design of an appropriate feeding strategy. Moreover, the use of the wine industry by-product showed promising results to support a continuing field-scale investigation/pilot-test assay.

5 ACKNOWLEDGMENTS

This study was supported by the projects REMEDIATION CGL2014-57215-C4-1-R, INDEMNE CGL2015-69768-R (MINECO/FEDER) and ACWAPUR PCIN-2015-239 from the Spanish Government, the project 2014SGR-1456 from the Catalan Government. The authors would like to thank the “Centres Científics i Tecnològics” of the “Universitat de Barcelona” for the chemical and isotopic analyses.

6 REFERENCES

Abongwa, P.T., Atekwana, E.A., 2013. Assessing the temporal evolution of dissolved inorganic carbon in waters exposed to atmospheric CO_2(g): A laboratory approach. J. Hydrol. 505, 250–265.

Akunna, J.C., Bizeau, C., Moletta, R., 1993. Nitrate and Nitrite Reductions with Anaerobic Sludge Using Various Carbon Sources: Glucose, Acetic Acid, Lactic Acid and Methanol. Water Res. 27, 1303–1312.

Abe, Y. and Hunkeler, D. (2006) Does the Rayleigh equation apply to evaluate field isotope data in contaminant. Environ. Sci. Technol. 40(5), 1588-1596.

Bielefeldt, A., McEachern, C. and Illangasekare, T. (2002) Hydrodynamic Changes in Sand due to Biogrowth on Naphthalene and Decane. J. Environ. Eng. 128(1), 51-59.

Blair, N., Leu, A., Munoz, E., Olsen, J., Kwong, E. and Des Marais, D. (1985) Carbon isotopic fractionation in heterotrophic microbial metabolism. Appl. Environ. Microbiol. 50(4), 996-1001.

Carles Brangarí, A., Sanchez-Vila, X., Freixa, A., M. Romaní, A., Rubol, S. and Fernàndez-Garcia, D. (2017) A mechanistic model (BCC-PSSICO) to predict changes in the hydraulic properties for bio-amended variably saturated soils. Water Resour. Res. 53(1), 93-109.

Carrey, R., Otero, N., Vidal-Gavilan, G., Ayora, C., Soler, A. and Gómez-Alday, J.J. (2014a) Induced nitrate attenuation by glucose in groundwater: Flow-through experiment. Chem. Geol. 370(0), 19-28.

Carrey, R., Rodríguez-Escales, P., Otero, N., Ayora, C., Soler, A. and Gómez-Alday, J.J. (2014b) Nitrate attenuation potential of hypersaline lake sediments in central Spain: Flow-through and batch experiments. J. Contam. Hydrol. 164(0), 323-337.

Coffin, R.B., Velinsky, D.J., Devereux, R., Price, W.A. and Cifuentes, L.A. (1990) Stable carbon isotope analysis of nucleic acids to trace sources of dissolved substrates used by estuarine bacteria. Appl. Environ. Microbiol. 56(7), 2012-2020.

Delay, F., Porel, G. and Chatelier, M. (2013) A dual flowing continuum approach to model denitrification experiments in porous media colonized by biofilms. J. Contam. Hydrol. 150(0), 12-24.

Fernández-Nava, Y., Marañón, E., Soons, J. and Castrillón, L. (2008) Denitrification of wastewater containing high nitrate and calcium concentrations. Bioresou. Technol. 99(17), 7976-7981.

Glass, C. and Silverstein, J. (1998) Denitrification kinetics of high nitrate concentration water: pH effect on inhibition and nitrite accumulation. Water Res. 32(3), 831-839.

Gómez, M.A., González-López, J. and Hontoria-García, E. (2000) Influence of carbon source on nitrate removal of contaminated groundwater in a denitrifying submerged filter. J. Hazard. Mater. 80(1–3), 69-80.

He, B., Kanae, S., Oki, T., Hirabayashi, Y., Yamashiki, Y. and Takara, K. (2011) Assessment of global nitrogen pollution in rivers using an integrated biogeochemical modeling framework. Water Res. 45(8), 2573-2586.

Khan, I.A. and Spalding, R.F. (2004) Enhanced in situ denitrification for a municipal well. Water Res. 38(14–15), 3382-3388.

Knowles, R. (1982) Denitrification. Microbiol. Rev. 46(1), 43-70.

Korom, S.F. (1992) Natural denitrification in the saturated zone: A review. Water Resour. Res. 98(6).

Martin, D., Salminen, J., Niemi, R., Heiskanen, I., Valve, J., Hellstén, P. and Nystén, H. (2009) Acetate and ethanol as potential enhancers of low temperature denitrification in soil contaminated by fur farms: A pilot-scale study. J. Hazard. Mater. 163(2–3), 1230-1238.

Orozco, A.M.F., Contreras, E.M. and Zaritzky, N.E. (2010) Cr(Vi) reduction capacity of activated sludge as affected by nitrogen and carbon sources, microbial acclimation and cell multiplication. J. Hazard. Mater. 176(1–3), 657-665.

Parkhurst, D.L. and Appelo, C.A.J. (1999) User's guide to PHREEQC (version 2) - a computer program for speciation, reaction-path, 1D-transport, and inverse geochemical calculations. 99-4259, W.-R.I.R. (ed), U.S. GEOLOGICAL SURVEY.

Peng, Y.-z., Ma, Y. and Wang, S.-y. (2007) Denitrification potential enhancement by addition of external carbon sources in a pre-denitrification process. J. Environ. Sci. 19(3), 284-289.

Petta, L., De Gisi, S., Casella, P., Farina, R., Notarnicola, M., (2017) Evaluationof the treatability of a winery distillery (vinasse) wastewater by UASB, anoxic-aerobic UF-MBR and chemical precipitation/adsorption. J. Environ. Management, 201, 177-189.

Porges, N., Jasewicz, L. and Hoover, S. (1956) Principles of biological oxidation. In biological treatment of sewage and industrial wastes., Reinhold. Publ., New York.

Prommer, H. and Post, V. (2010) A Reactive Multicomponent Transport Model for Saturated Porous Media. User's Manual. v2.10.

Rittmann, B.E. and McCarty, P.L. (2001) Environmental biotechnology : principles and applications, McGraw-Hill, cop. 2001.

Rivett, M.O., Buss, S.R., Morgan, P., Smith, J.W.N. and Bemment, C.D. (2008) Nitrate attenuation in groundwater: A review of biogeochemical controlling processes. Water Res. 42(16), 4215-4232.

Rodríguez-Escales, P., Folch, A., van Breukelen, B.M., Vidal-Gavilan, G. and Sanchez-Vila, X. (2016a) Modeling long term Enhanced in situ Biodenitrification and induced heterogeneity in column experiments under different feeding strategies. J. Hydrol. 538, 127-137.

Rodríguez-Escales, P., Folch, A., Vidal-Gavilan, G. and van Breukelen, B.M. (2016b) Modeling biogeochemical processes and isotope fractionation of enhanced in situ biodenitrification in a fractured aquifer. Chem. Geol. 425, 52-64.

Rodríguez-Escales, P., van Breukelen, B., Vidal-Gavilan, G., Soler, A. and Folch, A. (2014) Integrated modeling of biogeochemical reactions and associated isotope fractionations

at batch scale: A tool to monitor enhanced biodenitrification applications. Chem. Geol. 365(0), 20-29.

Saitoh, S., Iwasaki, K. and Yagi, O. (2003) Development of a most-probable-number method for enumerating denitrifying bacteria by using 96-well microtiter plates and an anaerobic culture system. Microbes Environ. 18(4), 210-215.

Tallec, G., Garnier, J., Billen, G. and Gousailles, M. (2008) Nitrous oxide emissions from denitrifying activated sludge of urban wastewater treatment plants, under anoxia and low oxygenation. Bioresour. Technol. 99(7), 2200-2209.

Tartakovsky, B., Millette, D., Delisle, S. and Guiot, S.R. (2002) Ethanol-sitimulated bioremediation of nitrate-contaminated grounwater. Ground Water Monit. R. 22(1), 9.

Taylor, S.W. and Jaffé, P.R. (1990) Biofilm growth and the related changes in the physical properties of a porous medium: 3. Dispersivity and model verification. Water Resour. Res. 26(9), 2171-2180.

Torrentó, C., Urmeneta, J., Otero, N., Soler, A., Viñas, M. and Cama, J. (2011) Enhanced denitrification in groundwater and sediments from a nitrate-contaminated aquifer after addition of pyrite. Chem. Geology. 287(1–2), 90-101.

van Breukelen, B.M. (2007) Extending the Rayleigh Equation to Allow Competing Isotope Fractionating Pathways to Improve Quantification of Biodegradation. Environ. Sci. Technol. 41(11), 4004-4010.

van Breukelen, B.M. and Prommer, H. (2008) Beyond the Rayleigh Equation: Reactive Transport Modeling of Isotope Fractionation Effects to Improve Quantification of Biodegradation. Environ. Sci. Technol. 42(7), 2457-2463.

Vidal-Gavilan, G., Carrey, R., Solanas, A. and Soler, A. (2014) Feeding strategies for groundwater enhanced biodenitrification in an alluvial aquifer: Chemical, microbial and isotope assessment of a 1D flow-through experiment. Sci.Total Environ. 494–495(0), 241-251.

Vidal-Gavilan, G., Folch, A., Otero, N., Solanas, A.M. and Soler, A. (2013) Isotope characterization of an in situ biodenitrification pilot-test in a fractured aquifer. Appl. Geochem. 32(0), 153-163.

Wreen, B.A., Venosa, A.D. (1996) Selective enumeration of aromatic and aliphatic hydrocarbon degrading bacteria by a most-probable number procedure. Can. J. Microbiol., 42, 252-258.

Zheng, C. and Wang, P.P. (1999) MT3DMS: A modular three-dimensional multispecies model for simulation of advection, dispersion and chemical reactions of contaminants in groundwater systems. Documentation and User's Guide, Contract Reo. SERDP-99-41., U.S. Army Eng. Res. and Dev. Cent., Vicksburg, Miss.

Figure captions

Figure 1. Conceptual model of carbon flow in enhanced denitrification.

Figure 2. Experimental data (points) and modeling results (lines) of a) ethanol and b) nitrate. The gray zone indicates the period when the system was stopped.

Figure 3. Experimental data (points) and modeling results (lines) of a) DOC and ethanol, b) DOC and endogenous carbon (DOC_{en}), c) dissolved inorganic carbon (DIC), and d) percentages of ethanol and DOC_{en} during the experiment. The gray zone indicates the period when the system was stopped.

Figure 4. Experimental data (points) and modeling results (lines) of $\delta^{13}C$-ethanol a) $\delta^{13}C$-DIC and b) $\delta^{13}C$- DOC_t. The gray zone indicates the period when the system was stopped.

Figure 5. Conceptual model of carbon flow in enhanced denitrification with calibrated isotopic fractionation values obtained for each C transformation. $\delta^{13}C_a$ is referred to the average experimental value of different carbon pools.

Figure 6. Rayleigh distillation model to obtain the isotopic fractionation of a) $\varepsilon^{13}C_{EtOH}$ (assuming all DOC is derived from ethanol oxidation) and b) $\varepsilon^{13}C_{DOCen}$ assuming all DOC is derived from biomass degradation and that there is no isotopic fractionation in the biomass degradation.

Table captions

Table 1. Average inflow water concentration during flow-through experiment.

Table 2. Processes, components and rates involved during denitrification and carbon isotopic fractionation.

Table 3. Model parameters used in the denitrification model.

Figure1

Click here to download high resolution image

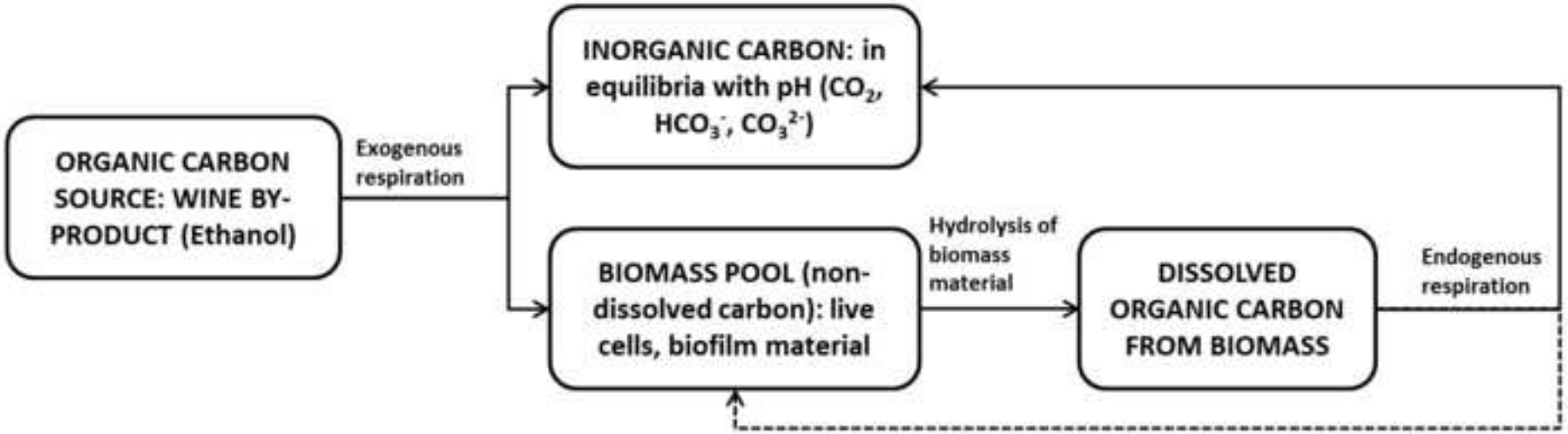

Figure2

Click here to download high resolution image

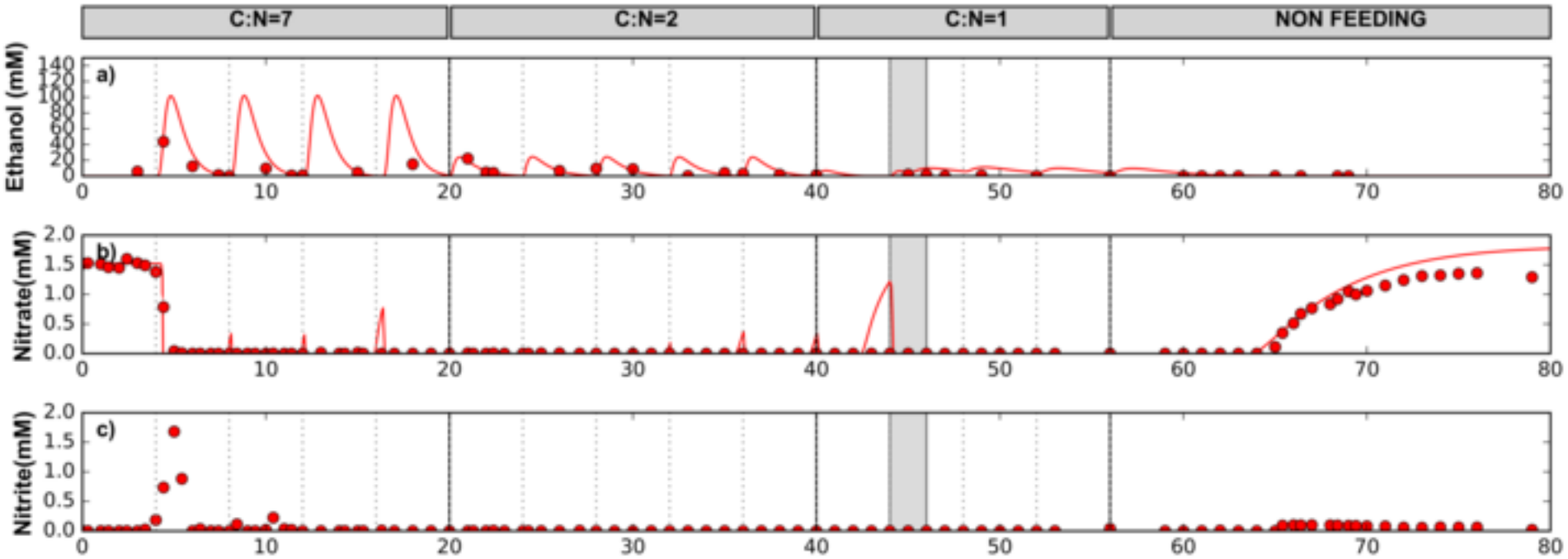

Figure3

Click here to download high resolution image

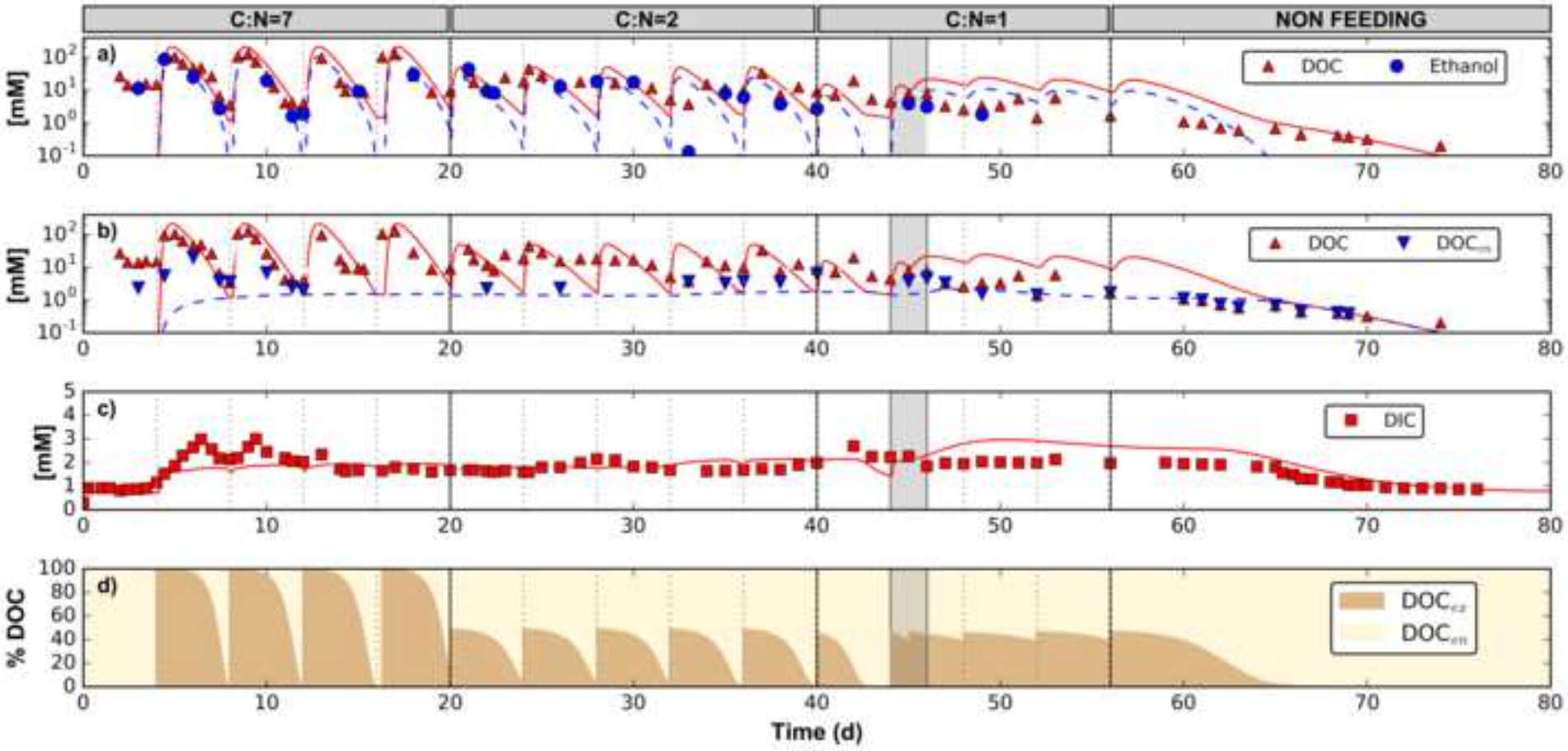

Figure4

Click here to download high resolution image

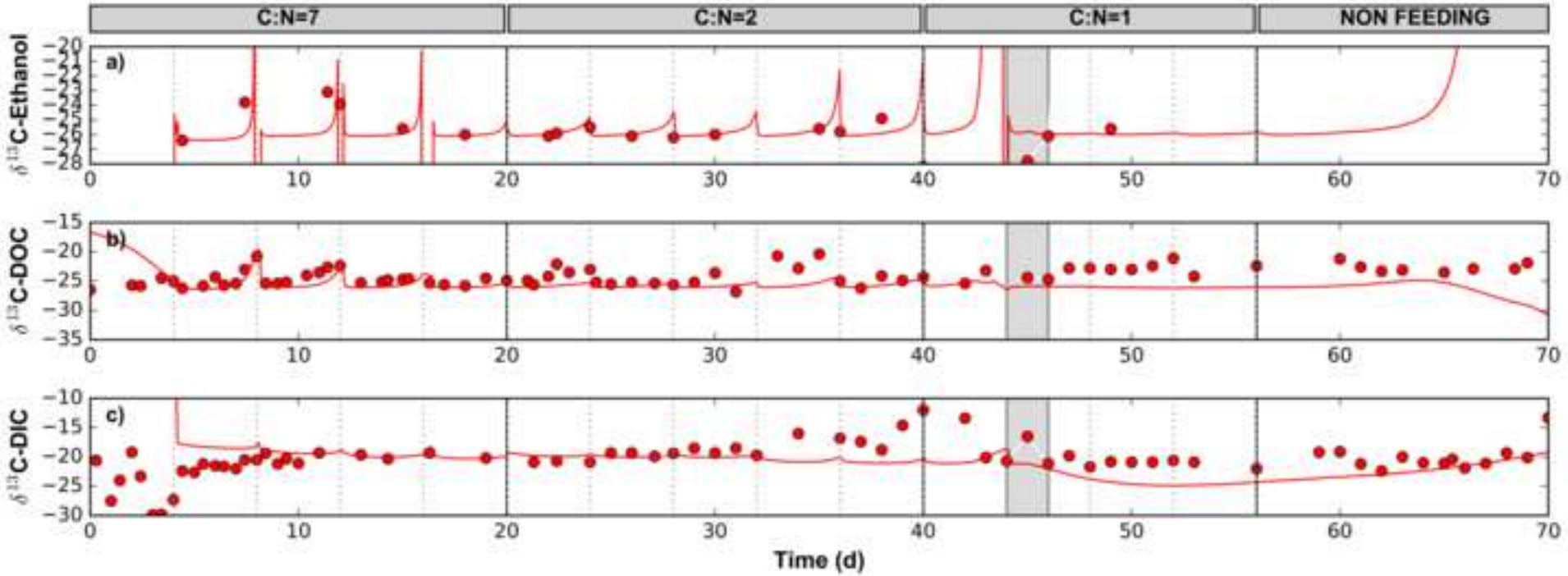

Figure5

Click here to download Figure: Figure 5.docx

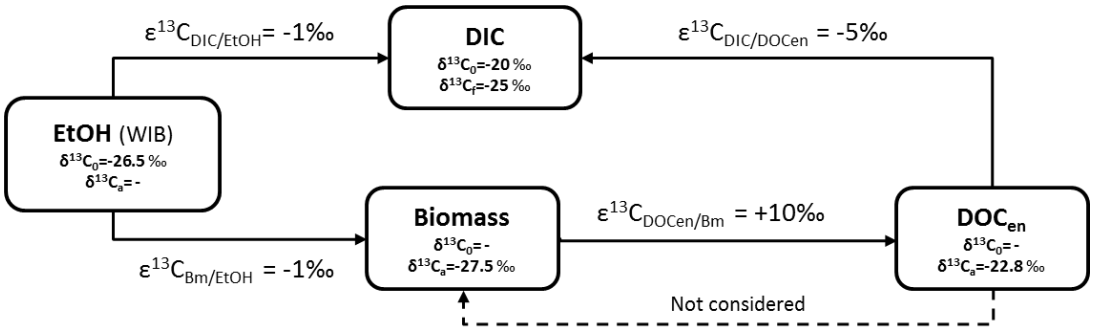

Figure6

Click here to download Figure: Figure 6.docx

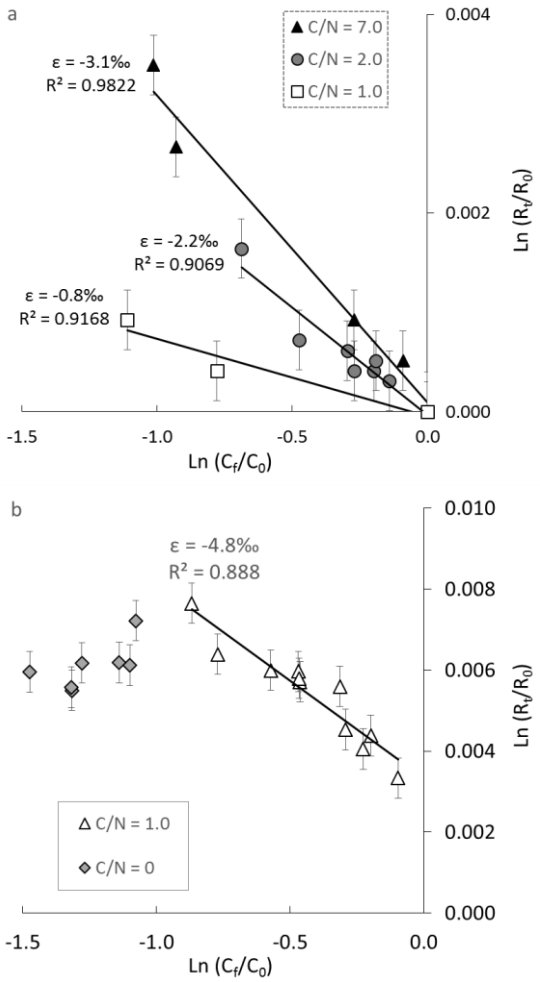

Table1

Click here to download Table: Table1.docx

	Na^+ (mM)	K^+ (mM)	Ca^{2+} (mM)	Mg^{2+} (mM)	Cl^- (mM)	NO_3^- (mM)	SO_4^{2-} (mM)	DIC (mM)	$\delta^{13}C_{DIC}$ (‰)	$\delta^{13}C_{EtOH}$ (‰)	pH	pe (mV)
Inflow water	6.62	1.08	0.91	1.29	5.46	1.72	2.28	0.51	-8.9	-26.1	6.2	+400

DIC: disolved inorganic carbón; pe: electron activity

Table2

Click here to download Table: Table2.docx

	Ethanol (EtOH)	DIC	Biomass (X)	DOC_{en}	$^{13}C_{EtOH}$	$^{13}C_{DIC}$	$^{13}C_{X}$	$^{13}C_{DOCen}$	Rates	
Oxidation of external electron donor	1	-P	$-Y_h$						$r_{EtOH} = -k_{max}\frac{[EtOH]}{[EtOH]+K_{S,EtOH}}\frac{[NO_3^-]}{[NO_3^-]+K_{S,NO_3^-}}[X]$	(1)
Biomass hydrolysis			1	-1					$r_X = -b[X]$	(2)
Oxidation of endogenous DOC		-1		1					$r_{DOC} = -K_1[DOC_{en}]$	(3)
Enrichment of external electron donor due to oxidation					1	-P	$-Y_h$		$r_{^{13}C_{EtOH}} = r_{EtOH}\left(\frac{\varepsilon_1}{1000}+1\right)\frac{[^{13}C_{EtOH}]}{[EtOH]}$	(4)
Enrichment of biomass due to hydrolysis							-1	1	$r_{^{13}C_X} = r_X\left(\frac{\varepsilon_2}{1000}+1\right)\frac{[^{13}C_X]}{[X]}$	(5)
Enrichment of endogenous DOC due to oxidation						1		-1	$r_{^{13}C_{DOC_{en}}} = r_{DOC_{en}}\left(\frac{\varepsilon_3}{1000}+1\right)\frac{[^{13}C_{DOC_{en}}]}{[DOC_{en}]}$	(6)

k_{max} : the consumption rate of electron donor per unit value of biomass [T^{-1}]

$K_{S,EtOH}$: half saturation constants of Ethanol [ML^{-3}]

K_{S,NO_3^-} : half saturation constants of nitrate [ML^{-3}]

DIC: Dissolved inorganic carbon

DOC_{en}: Endogenous non purgeable dissolved organic carbon

b : biomass decay constant [T^{-1}]

K_1 : first order degradation constant of oxidation of DOC_{en} [T^{-1}]

Y_h, P: stoichiometric parameters determined using equation (3).

ε : enrichment isotopic factor

Table3

Click here to download Table: Table3.docx

Parameter	Unit	This work	Literature values	References[a]
k_{max}	$[Md^{-1}]$	$9.5x10^{2}$	1×10^{1}; 1.1×10^{1}; $2x10^{1}$; $1.08x10^{2}$	1,2,3,4
$K_{S,NO3}$ (nitrate)	[M]	$1.0x10^{-6}$	1.6×10^{-6} ; 3.2×10^{-6} ; 1.2×10^{-5} ; 1.8×10^{-4}	1,3,2,4
$K_{S,DOC}$ (ethanol)	[M]	$1.0x10^{-5}$	8.3×10^{-6} ; 1.7×10^{-4} ; $6.6x10^{-4}$; 7.3×10^{-2}	1,2,3,4
b	d^{-1}	$3.0x10^{-1}$	$6x10^{-2}$; $1.5x10^{-1}$; $2x10^{-1}$	2,4,3
K_1	d^{-1}	$2.0x10^{-1}$	Not found	
ε_1	‰	-1	+8(*)	4
ε_2	‰	+10	Not found	
ε_3	‰	-5	Not found	

[a] References are 1, Chen and MacQuarrie (2004); 2, Lee et al., (2009); 3, Kinzelbach et al., (1991); 4, Rodríguez-Escales et al., (2014). (*) This value only considered the oxidation of ethanol into dissolved inorganic carbon, withouth the generation of endogenous organic carbon.

k_{max}: the consumption rate of electron donor per unit value of biomass; **$K_{S,DOC}$**: half saturation constants of dissolved organic carbon; **$K_{S,NO3}$**: half saturation constants of nitrate; **b**: biomass decay constant; **K_1**: first order degradation constant of oxidation of endogenous non purgeable dissolved organic carbon; **$\varepsilon_{1,2,3}$**: enrichment isotopic factor of ethanol, biomass and endogenous non purgeable dissolved organic carbon respectively